

Physical and observational constraints on the anvil cloud area feedback

Brett A. McKim^{*a,b}, Sandrine Bony^a, & Jean-Louis Dufresne^a

Abstract Changes in anvil cloud area with warming are a leading source of uncertainty in estimating the Earth’s climate sensitivity (1). Most approaches to bounding this area feedback rely on climate models or expert assessment. Here, we use observations and theory, a “storyline approach”, to bound it. We first derive a simple but quantitative expression for the anvil area feedback, which is shown to depend on the present day, measurable cloud radiative effects and the fractional change in anvil area with warming. Satellite observations suggest an anvil cloud radiative effect of about $\pm 1 \text{ Wm}^{-2}$, which requires the fractional change in anvil area to be about $\mp 50\% \text{ K}^{-1}$ to produce a feedback equal to its present-day lower bound. We use theory and observations to show that the change in anvil area is closer to about $-4\% \text{ K}^{-1}$. This rules out the previous estimate of the area feedback and leads to our new estimate of $0.02 \pm 0.07 \text{ Wm}^{-2} \text{ K}^{-1}$, which is many times weaker and more constrained. In comparison, we show the anvil cloudy albedo feedback to be much less constrained. This poses an obstacle for bounding the Earth’s climate sensitivity.

EARTH’S climate sensitivity is closely linked to the strength of cloud feedbacks. Although this has long been recognized (2–4), understanding and quantifying cloud feedbacks has proved difficult and sometimes controversial (5–12). Anvil clouds pose a particular challenge because their near neutral radiative balance results from large yet opposing radiative effects (13). Is this balance guaranteed? Or will warming tip the scales?

Uncertainty around anvil cloud feedbacks

Ramanathan and Collins (5) were the first to study the anvil cloud area feedback. Observing the coincident drop off in frequency of deep convection and surface temperature above a critical temperature, they hypothesized that anvils regulate the underlying surface temperatures. However, their observation is no longer considered evidence of a tropical thermostat (6, 14–16).

Years later, Lindzen et al (7) hypothesized that if cirrus cover were to decrease with warming, perhaps due to microphysical effects, it would act like an iris, significantly inhibiting further warming. Criticism of this work’s methodology soon followed (8, 17, 18), but it did not rule out the existence of a strong area feedback.

Anvil clouds are controlled in part by unconstrained microphysics (19–21), but they are also controlled by robust thermodynamic principles (22, 23). These principles predict that anvils decrease in area with warming because the static stability of the atmosphere increases (24), which is consistent with observed variability (25–27) and with most simulations (28). Despite growing confidence in this aspect of climate change, comprehensive assessments consider the anvil cloud area feedback to be a leading source of uncertainty in estimating climate sensitivity (1, 29).

This mismatch in confidence and uncertainty might appear inconsistent, but what is called the anvil cloud area feedback is in fact the result of two types of changes in anvil clouds: an area change and an optical depth change. These changes are usually convolved in feedback decompositions (1, 29, 30), so the question of which feedback truly embodies the uncertainty remains unanswered. This calls for the need to separate them and settle which process poses the main obstacle to constraining the Earth’s climate sensitivity.

Qualitative arguments suggest that the area feedback should be small because anvils are radiatively neutral (6, 31, 32). But how neutral must anvil clouds be for their area feedback to be insignificant? What if their cloud radiative effect changes with warming? And what if when anvils shrink, more of the Earth is exposed to the radiative effects and feedbacks of underlying low clouds?

Optical depth controls an anvil’s cloudy albedo (reflectivity independent of cloud fraction). Qualitative arguments suggest that changes in optical depth might produce a stronger cloudy albedo feedback because anvils have a much stronger shortwave effect than in the net (31). But how much does cloudy albedo change with warming? And how much must it change to produce a substantial feedback?

Clearing the cloud of uncertainty A physically-motivated decomposition that distinguishes the anvil area feedback from the anvil cloudy albedo feedback is needed. Since models must contend with representing unconstrained microphysics (19–21), we prefer to use observations. This requires a decomposition that can relate observable cloud properties to cloud feedbacks in a transparent way. We want to avoid the persistent confusions that exist for cloud feedbacks (33), even for the well-known anvil altitude feedback (12).

To achieve these goals, we will derive a novel, analytical cloud feedback decomposition based on the essential physics of cloud radiative effects. When combined with observations, this decomposition lets us identify, understand, and quantitatively constrain cloud feedbacks in a physically transparent way.

Compiled on 27 May 2023

* Corresponding author address: bam218@exeter.ac.uk

^a LMD/IPSL, Sorbonne Université, CNRS, 75252 Paris, France

^b University of Exeter, Stocker Rd, EX4 4PY Exeter, UK

We will adopt a ‘storyline approach’ (34), in which we examine the driving factors that control a cloud feedback and determine the plausibility of these factors to produce a particular feedback value. For example if the current lower bound of $-0.4 \text{ Wm}^{-2}\text{K}^{-1}$ for the area feedback (29) requires a large change in cloud area, but the expected change in cloud area is much smaller, then this feedback value can be ruled out. We will use this storyline approach to show which feedback is constrained and which is the obstacle to constraining climate sensitivity.

Conceptualizing cloud radiative effects

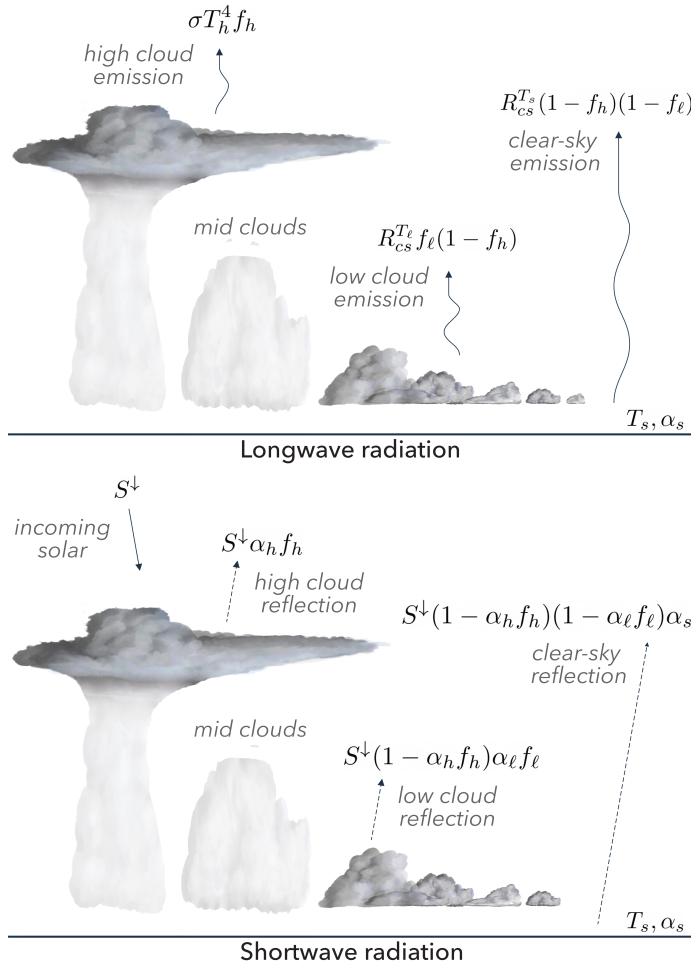


Figure 1: *Conceptualizing cloud radiative effects.* We idealize the vertical cloud profile into two distinct layers that represent anvil clouds and low clouds with random overlap. Equations indicate the domain-averaged contribution of high clouds, low clouds, and the surface to TOA energy balance. Their sum in the longwave and shortwave is given by Equation 13 and 15, respectively. See Table 1 for symbol meanings and values.

Clouds are complex, but for simplicity we divide them into two types: high (h) and low (ℓ). (Considering mid-level clouds does not change our conclusions.) We subsume their properties into a few bulk parameters that can be obtained from observations and reanalysis (Table 1). These properties include their area fraction f_h, f_ℓ , their emission temperature T_h, T_ℓ , and their cloudy albedo α_h, α_ℓ (which is

independent of cloud fraction). Clear-sky radiation can also be distilled into a few parameters: the incoming solar radiation S^\downarrow , the surface albedo α_s , and the outgoing longwave radiation for a given surface temperature $R_{cs}^{T_s}$. This simplification permits the derivation of analytical expressions for cloud radiative effects from high clouds and low clouds C_h, C_ℓ ; cloud overlap effects $m_{\ell h}$; and the TOA energy balance N . See Figure 1 for an illustration and Methods for the derivation.

Analytic feedbacks and the storyline approach

Feedbacks are computed by differentiating Earth’s TOA energy balance (Equation 15 minus Equation 13, see Methods) with respect to the surface temperature T_s (35). To start, we have:

$$\lambda \equiv \frac{dN}{dT_s} = \frac{dN_{cs}}{dT_s} + \frac{dC}{dT_s}, \quad (1)$$

where N_{cs} is the clear-sky TOA energy balance and $C = C_h + C_\ell + m_{\ell h}$ is the net cloud radiative effect from all clouds. Plugging in the analytical expressions for C (Equation 14 and 16, see Methods), we arrive at an equation for tropical climate feedbacks in terms of our bulk parameters:

$$\lambda = \lambda_0 + \sum_{i=h,\ell} \left(\lambda_i^{\text{area}} + \lambda_i^{\text{temp}} + \lambda_i^{\text{albedo}} \right), \quad (2)$$

where λ_0 is the reference response assuming a fixed anvil temperature and fixed relative humidity (12, 36); and λ_i^{area} , λ_i^{temp} , $\lambda_i^{\text{albedo}}$ are the feedbacks from changes in cloud area, cloud temperature, and cloudy albedo with warming. All feedbacks are described analytically. See Methods for the full derivation.

These analytic expressions form the basis of our storyline approach by transparently and quantitatively relating changes in cloud properties to their resulting radiative feedbacks. Let us first focus on the high cloud area feedback, λ_h^{area} .

The anvil cloud area feedback After collecting all terms from Equation 1 that involve changes in anvil area df_h/dT_s , we arrive at a remarkably simple equation for the anvil cloud area feedback,

$$\lambda_h^{\text{area}} = \frac{d \ln f_h}{dT_s} (C_h + m_{\ell h}). \quad (3)$$

It depends on the *fractional* change in anvil area with warming $d \ln f_h/dT_s$ and the sum of the *present day* anvil cloud radiative effect C_h and cloud overlap effect $m_{\ell h}$. The logarithmic derivative is used, not only because it follows from the algebra, but also because fractional changes in cloud area are easier to interpret and bound than absolute changes—as we will soon see. And though we computed the change in cloud radiative effect with warming, the area feedback does not depend on the change in radiative effect, but its present-day value. This means it can be measured and used to constrain the feedback.

Table 1: *Climatological values of tropical quantities (30°S – 30°N) used in this study.* All radiative quantities are evaluated at the top of atmosphere. C_{obs}^{lw} and C_{obs}^{sw} refer to the observed longwave and shortwave cloud radiative effects from CERES. See Climatology section for details.

| Quantity | Description | Tropical mean value | Derivation |
|----------------|----------------------------------|------------------------|-----------------------------------|
| f_h | Anvil cloud area fraction | 0.17 | CALIPSO |
| f_ℓ | Low cloud area fraction | 0.10 | CALIPSO |
| T_h | Anvil temperature | 221 K | ERA5 |
| T_ℓ | Low cloud temperature | 287 K | ERA5 |
| T_s | Surface temperature | 298 K | HadCRUT5 |
| α_s | Surface albedo | 0.13 | CERES |
| S^\downarrow | Incoming shortwave radiation | 398 Wm^{-2} | CERES |
| S_{cs} | Clear-sky absorbed shortwave | 347 Wm^{-2} | CERES |
| R_{cs} | Clear-sky outgoing longwave | 287 Wm^{-2} | CERES |
| n | Effective cloud fraction scaling | 1.7 | Fitted from C_{obs}^{lw} |
| α_h | Anvil albedo | 0.45 | Fitted from C_{obs}^{sw} |
| α_ℓ | Low cloud albedo | 0.45 | Fitted from C_{obs}^{sw} |
| C | Net cloud radiative effect | -14.8 Wm^{-2} | Inferred |
| C^{sw} | Shortwave cloud radiative effect | -41.8 Wm^{-2} | Inferred |
| C^{lw} | Longwave cloud radiative effect | 27.0 Wm^{-2} | Inferred |
| C_h | Anvil cloud radiative Effect | -2.0 Wm^{-2} | Inferred |
| C_ℓ | Low cloud radiative effect | -13.4 Wm^{-2} | Inferred |
| $m_{\ell h}$ | Cloud overlap effect | 0.5 Wm^{-2} | Inferred |

137 **The storyline approach in a nutshell** Equation 3 reveals
138 that the smaller the climatological anvil cloud radiative effect,
139 the larger the change in anvil area would have to be
140 to produce a given feedback strength. Therefore, we can
141 probe the plausibility of a particular strength by first quan-
142 tifying the observed anvil cloud radiative effect; then calcu-
143 lating the change in anvil area required to produce such a
144 feedback strength; and then comparing the required change
145 in anvil area to the amount expected from theory, simu-
146 lations, and observations. If the expected change in anvil
147 area is much smaller than the required change, then that
148 particular feedback strength can be ruled out.

149 Climatology

150 Bounding the area feedback beyond $\lambda_h^{\text{area}} = -0.2 \pm 0.2$
151 $\text{Wm}^{-2} \text{K}^{-1}$ (29) with the storyline approach requires quan-
152 tifying the tropically averaged anvil cloud radiative effect
153 and cloud overlap effect ($C_h + m_{\ell h}$). Since these quantities
154 are not directly observed, they will be inferred from our
155 simple model of cloud radiative effects.

156 We do this by inputting observations of cloud fraction
157 from CALIPSO (37), clear-sky radiation from CERES (38),
158 surface temperature from HadCRUT5 (39), and atmo-
159 spheric temperature from ERA5 reanalysis (40) into our
160 expression for the net cloud radiative effect (Equations 14
161 and 16), see Methods. f_h and f_ℓ are identified as the maxi-
162 mum of the observed cloud fraction profile above 8 km and
163 below 4 km, respectively. We then ensure goodness of fit
164 with between the inferred and the observed cloud radi-
165 ative effects by treating the effective cloud fraction scaling
166 n (which accounts for collapsing the anvil cloud fraction
167 profile into a single level, see Methods and Extended Data

Figure 1) and the cloud albedo of anvil cloud and low clouds
as tuneable parameters. 168

169 We test our idealizations by comparing the observed net,
170 shortwave, and longwave cloud radiative effects (C_{obs} , C_{obs}^{sw} ,
171 C_{obs}^{lw}) with their counterparts from the simple model (Fig-
172 ure 2), which take the spatial fields of cloud fraction, tem-
173 perature, albedo, and clear-sky radiation as inputs. Our
174 model can reproduce the spatial patterns of longwave and
175 shortwave cloud radiative effects, although there are small
176 deviations throughout the tropics, such as an underestimate
177 of C in the south east of China and an overestimate of C
178 in the eastern Pacific, next to South America (Figure 2c).
179 Given the overall close agreement, we consider our model
180 fit for the task of evaluating the anvil cloud area feedback.
181

182 The climatological values of tropical quantities used in
183 our calculations are summarized in Table 1 and the cloud
184 properties of interest are plotted in Figure 3. f_h is maxi-
185 mum in the West Pacific Warm Pool and f_ℓ is maximum
186 along the East Pacific. Decomposing C into its contribu-
187 tions from different layers reveals that the net C is domi-
188 nated by C_ℓ . By comparison, the overlap effect $m_{\ell h}$ is much
189 smaller and varies less. The same is true for the high cloud
190 radiative effect C_h , which exhibits a remarkable cancellation
191 between its shortwave and longwave components not just in
192 the warm pool (13, 27, 41–44), but across the tropics.

193 Ruling out the lower bound

194 With these more precise values in hand, we can constrain
195 the tropical anvil cloud area feedback. To scale our estimate
196 of λ_h^{area} to the global average, we multiply by the area ratio
197 of the tropics and the globe, 1/2.

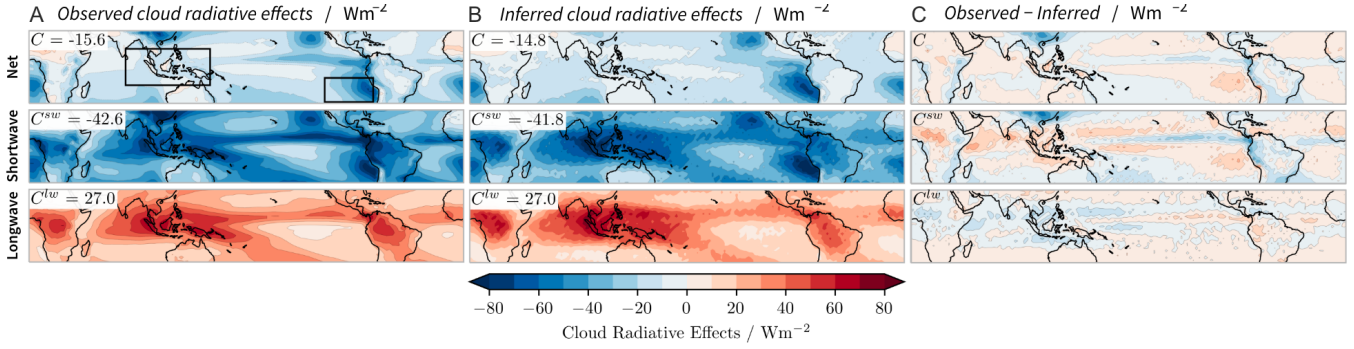


Figure 2: Observed net, shortwave, and longwave cloud radiative effects (C , C^{sw} , C^{lw}) from CERES compared to their inferred counterparts. Tropical mean values are shown in the upper left of each panel. The West Pacific Warm Pool and East Pacific regions are boxed in a). The colorbar is the same for all plots.

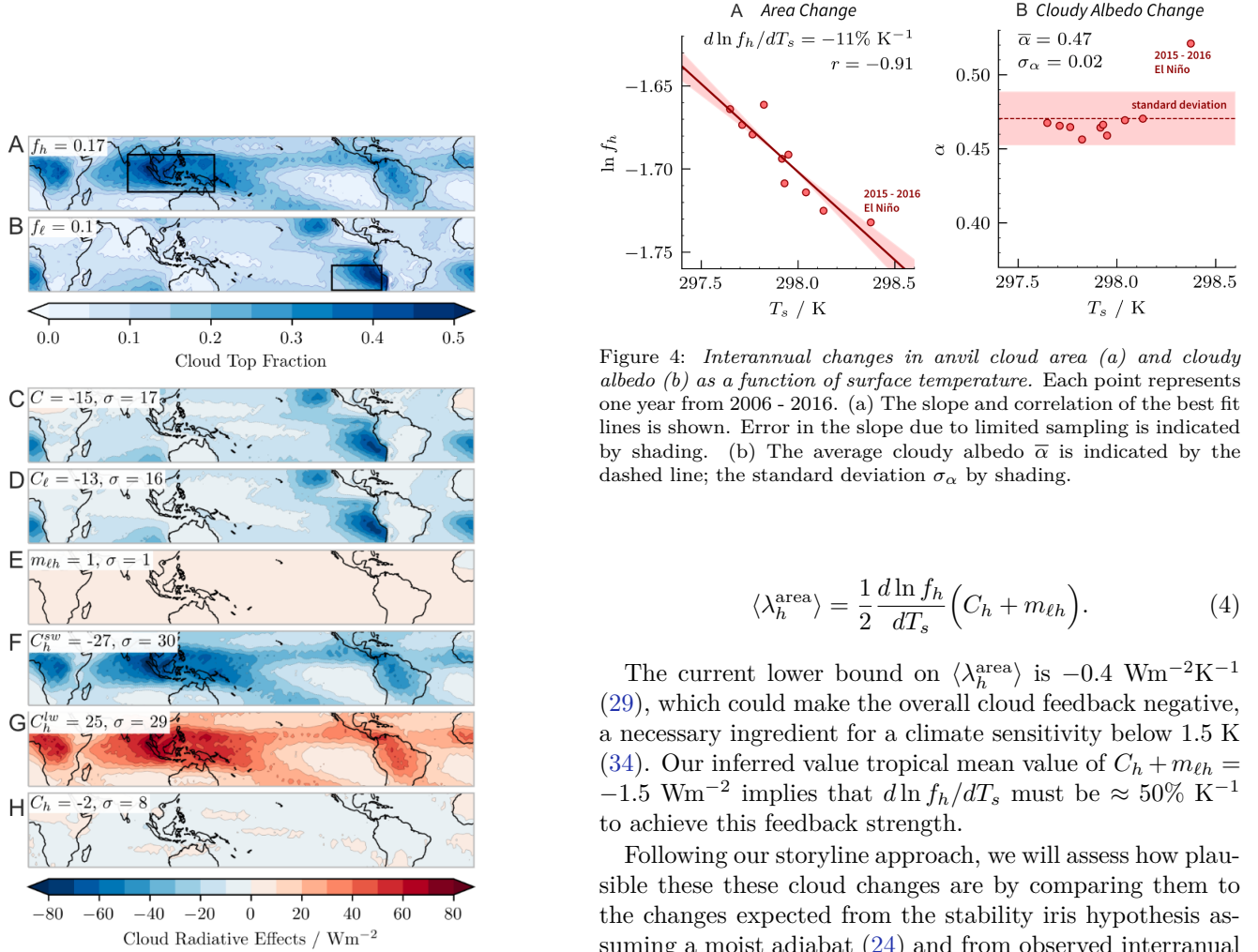


Figure 3: Climatological values of tropical quantities. a) Effective anvil cloud fraction and b) low cloud fraction from CALIPSO. The West Pacific Warm Pool and East Pacific regions are boxed to indicate regions of maximum anvil and low cloud coverage, respectively. c-h) Inferred cloud radiative effects from Equations 17, 18, 20. Tropical mean values and standard deviations are shown in the upper left of each panel. Refer to Extended Data Figure 2 to see m_{lh} and C_h plotted with a finer color scale.

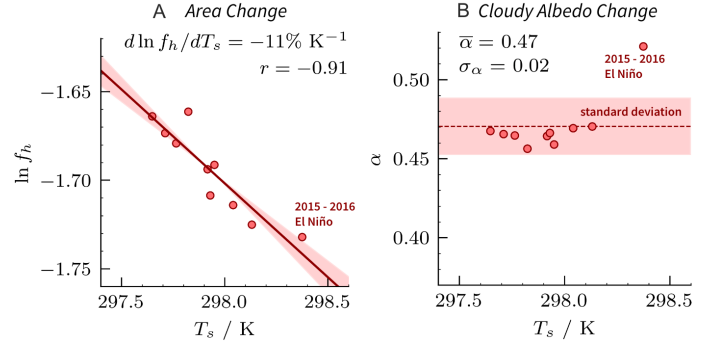


Figure 4: Interannual changes in anvil cloud area (a) and cloudy albedo (b) as a function of surface temperature. Each point represents one year from 2006 - 2016. (a) The slope and correlation of the best fit lines is shown. Error in the slope due to limited sampling is indicated by shading. (b) The average cloudy albedo $\bar{\alpha}$ is indicated by the dashed line; the standard deviation σ_α by shading.

$$\langle \lambda_h^{\text{area}} \rangle = \frac{1}{2} \frac{d \ln f_h}{dT_s} (C_h + m_{lh}). \quad (4)$$

The current lower bound on $\langle \lambda_h^{\text{area}} \rangle$ is $-0.4 \text{ Wm}^{-2}\text{K}^{-1}$ (29), which could make the overall cloud feedback negative, a necessary ingredient for a climate sensitivity below 1.5 K (34). Our inferred value tropical mean value of $C_h + m_{lh} = -1.5 \text{ Wm}^{-2}$ implies that $d \ln f_h / dT_s$ must be $\approx 50\% \text{ K}^{-1}$ to achieve this feedback strength.

Following our storyline approach, we will assess how plausible these these cloud changes are by comparing them to the changes expected from the stability iris hypothesis assuming a moist adiabat (24) and from observed interannual variability (25).

Changes in anvil area with warming The stability iris hypothesis (24) states that the anvil cloud fraction f_h is proportional to detrainment from deep convection. Owing to mass conservation, this detrainment is equal to the clear-sky convergence, $\partial_p \omega$, where ω is the subsidence vertical velocity [hPa/day]. If we make the ansatz that $\partial_p \omega$ is proportional to ω at the level of detrainment (h), then the fractional change in anvil area is equal to the fractional change in subsidence velocity at the anvil level:

$$\frac{d \ln f_h}{dT_s} = \frac{d \ln \omega_h}{dT_s}. \quad (5)$$

The subsidence velocity can be written as the quotient of the clear-sky radiative flux divergence in temperature coordinates ($-\partial_T F$) and the difference between the actual and dry lapse rates (21):

$$\omega = \frac{-\partial_T F}{1/\Gamma - 1/\Gamma_d}. \quad (6)$$

Given that $\partial_T F$ does not vary with surface temperature (45), if we further assume that Γ_h , the lapse rate at the anvil level, is moist adiabatic, then the change in cloud area can be computed with a few representative numbers. Assuming the surface warms from $T_s = 298$ K to 299 K and the anvil cloud warms from $T_h = 221$ K to anywhere between 221 and 221.4 K (a typical range of anvil warming, see 46 and references therein), then we expect that anvils change in area at about,

$$\begin{aligned} \frac{d \ln f_h}{dT_s} &= -\frac{d \ln(1/\Gamma_h - 1/\Gamma_d)}{dT_s} \quad (\text{stability iris}) \\ &\approx -1 \text{ to } -4\% \text{ K}^{-1}, \end{aligned} \quad (7)$$

depending on the amount of anvil warming. Despite the numerous simplifications in our derivation, the result is similar to the range produced by cloud resolving models (28).

Now turning to ENSO-driven interannual variability, we compute annual averages of $\ln f_h$ and T_s (the tropical mean surface temperature) from July to June, similar to (25). To avoid logarithmic divergences, we exclude grid cells with $f_h = 0$. We scatter annual averages of $\ln f_h$ against T_s in Figure 4. The line of best fit for this relation gives

$$\frac{d \ln f_h}{dT_s} \approx -11\% \text{ K}^{-1}. \quad (\text{interannual variability}) \quad (8)$$

Since both of these estimates of anvil cloud changes are much smaller than what is required to achieve the lower bound on $\langle \lambda_h^{\text{area}} \rangle$ (29), the area feedback assessment should be revised.

Best estimate of the area feedback Care should be taken when determining the anvil cloud area change with warming on different timescales. Anvil area is better correlated with upper tropospheric stability than surface temperature (25, 26), and surface- and upper-tropospheric warming (and thus changes in stability $1/\Gamma_h - 1/\Gamma_d$) do not always go hand-in-hand on interannual timescales (47, 48). This may alter the anvil area sensitivity to surface temperature inferred from variability. Indeed, the IPSL general circulation model (GCM) suggests that anvil clouds are about half as sensitive for long term warming as compared to interannual variability (26). Furthermore, ENSO-driven interannual variability is not only associated with a change in surface temperature, but also a reorganization of deep convection from the West Pacific to the Central Pacific (49)

which may further alter the inferred relationship between anvil area and surface temperature on different timescales.

Given the evidence from theory assuming a moist-adiabatic change in lapse rate (Equation 7), observations of interannual variability (Equation 8), and simulations (26, 28), we estimate that the anvil cloud area changes at about

$$\frac{d \ln f_h}{dT_s} = -4 \pm 2\% \text{ K}^{-1}. \quad (\text{best estimate}) \quad (9)$$

We found $C_h + m_{\ell h} = -1.5 \text{ Wm}^{-2}$, but other observational studies have estimated -4 Wm^{-2} (44), 0.6 Wm^{-2} (19), and 2 Wm^{-2} (50). This is probably due to methodological differences and the fact that anvil clouds have no precise definition. Furthermore, CERES TOA fluxes have an uncertainty of 2.5 Wm^{-2} (38). Considering mid-level clouds adds an additional uncertainty of 0.5 Wm^{-2} (see Methods). Therefore, we estimate the anvil cloud radiative effect and cloud overlap effect to be,

$$C_h + m_{\ell h} = -1 \pm 3 \text{ Wm}^{-2}. \quad (\text{best estimate}) \quad (10)$$

Using these best estimates in Equation 4, we get our best estimate of the anvil area feedback to within one standard deviation:

$$\langle \lambda_h^{\text{area}} \rangle = 0.02 \pm 0.07 \text{ Wm}^{-2} \text{ K}^{-1}. \quad (\text{best estimate}) \quad (11)$$

Our estimate for the anvil cloud area feedback is positive but ten times smaller in magnitude and three times more constrained than the WCRP estimate of $-0.2 \pm 0.2 \text{ Wm}^{-2} \text{ K}^{-1}$ (29). We deem that the area feedback is now well constrained because its uncertainty is comparable to other cloud feedbacks (1, 29). What about the anvil cloudy albedo feedback?

Uncertainty in the anvil cloudy albedo feedback

Qualitative arguments suggest a significant feedback could be produced without any change in anvil area (31), but let us make that notion quantitative by considering our analytical expression for the anvil cloudy albedo feedback,

$$\lambda_h^{\text{albedo}} = \frac{1}{2} \frac{d \ln \alpha_h}{dT_s} (C_h^{sw} + m_{\ell h}^{sw}). \quad (12)$$

It follows a similar form to the area feedback but depends on the fractional change in cloudy albedo with warming $d \ln \alpha_h / dT_s$, the shortwave anvil cloud radiative effect C_h^{sw} , and the shortwave cloud overlap effect $m_{\ell h}$.

Given that $C_h^{sw} + m_{\ell h}^{sw}$ is about -25 Wm^{-2} (Figure 3f), producing a feedback of $-0.2 \text{ Wm}^{-2} \text{ K}^{-1}$ requires a fractional change in cloudy albedo of only 1 to 2% K^{-1} . In contrast to anvil area, even a small change in the anvil's cloudy albedo could produce a strong radiative response. The plausibility of such a change is unclear.

On the one hand, the cloudy albedo might decrease if the optically thick portion of anvils decrease with warming more than thin portions, as suggested by variability

(51). On the other hand, it might increase if anvils contain more condensate with warming, as could happen if precipitation efficiency remains constant (24). Building a more sophisticated theory of cloud condensate, perhaps based on a bulk plume model (52, 53), could help make quantitative, testable predictions that focus future research.

Up to this point, all of the inferred climatology has been calculated assuming a constant cloudy albedo (α) that is identical for anvils and low clouds over the 2006 - 2016 period (see Methods). If we now compute α for each year, we find that it exhibits no clear trend with warming, although it significantly increases during the 2015 - 2016 El Niño (Figure 4b). This is interesting in its own right, but given that low clouds might increase their cloudy albedo independently of anvils (54), distinguishing α_h from α_ℓ will be required to make firmer conclusions.

A 1 to 2 % K^{-1} change in cloudy albedo cannot be dismissed, so we conclude that the uncertainty in previous assessments of anvil clouds (1, 29) is embodied by the cloudy albedo feedback.

Discussion

Summary We have developed a feedback decomposition that can transparently disentangle feedbacks from changes in the area and the cloudy albedo of anvil clouds.

We showed that the anvil cloud area feedback is constrained by the present day cloud radiative effect and not by the unrealized change in cloud radiative effect with warming. Since anvil clouds are radiatively neutral at present ($C_h = -2 \text{ Wm}^{-2}$), an anvil cloud area feedback equal to that derived from comprehensive assessments ($-0.2 \text{ Wm}^{-2}\text{K}^{-1}$, 1, 29) requires implausibly large changes in anvil area. Overlap effects with low-level clouds are accounted for ($m_{\ell h} = 0.5 \text{ Wm}^{-2}$). They dampen the anvil cloud area feedback by about 25%, but do not qualitatively change our conclusions. Our results provide a theoretical and observational basis for previously qualitative arguments.

The anvil cloudy albedo feedback, which is often obscured in feedback decompositions, is constrained by the present day shortwave cloud radiative effect. Since anvils are strongly reflective ($C_h^{sw} + m_{\ell h}^{sw} = -25 \text{ Wm}^{-2}$), an anvil cloudy albedo feedback of $-0.2 \text{ Wm}^{-2}\text{K}^{-1}$ requires a fractional change in cloudy albedo of only 1 to 2 % K^{-1} , but the plausibility of such a change remain unclear. This presents an obstacle for bounding the Earth's climate sensitivity.

Lingering questions A limitation of our study is that our decomposition neglects cloud-moisture coupling and the fact that anvils are composed of clouds with many optical depths and opposing radiative effects (55). Untangling these contributions to the area feedback is not only a technical challenge but a conceptual one, as the following questions demonstrate:

Why is the anvil cloud radiative effect so close to zero? Given the continuum spectrum of anvil cloud optical thickness (55), radiative neutrality might be a coincidence (43),

or some stabilization principle could be at work (44, 56). We have shown that the anvil area feedback is a function of the present anvil cloud radiative effect, so the feedback is state dependent and could vary between climates if the radiative effect changes. Understanding why $C_h \approx 0 \text{ Wm}^{-2}$ would also help to constrain the anvil cloudy albedo feedback.

What is the feedback from mesoscale deep-convective aggregation? Increased aggregation can decrease anvil area and dry out the atmosphere (57-59). Since we have shown that changes in anvil cloud area are not a significant feedback, the radiative feedbacks associated with aggregation may instead come from changes in humidity or cloudy albedo. There are indeed observable changes in N and N_{cs} due to the aggregation of deep convection (57, 59), but properly quantifying the radiative feedbacks from humidity and anvil changes has yet to be carried out.

Conclusions The big picture from our work is that theory and observations can be used to not only understand, but quantitatively constrain aspects of climate change. This is a boon for phenomenon that are difficult to simulate.

We use this approach to constrain the anvil cloud area feedback. But in closing one door, we open another. The relative theoretical and observational uncertainty of the anvil cloudy albedo feedback demands focused attention but promises enhanced returns for constraining climate sensitivity.

With regards to generality, it might be possible to constrain other cloud feedbacks through a similar approach. Our feedback expressions might also provide a quick, quantitative, and physically transparent way to interpret how model biases influence feedbacks. For instance, if members of a GCM ensemble simulate C_h between $\pm 10 \text{ Wm}^{-2}$, but they all simulate the same $d \ln f_h / dT_s = -4 \% \text{ K}^{-1}$, then their area feedbacks will range between $\mp 0.2 \text{ Wm}^{-2}\text{K}^{-1}$. If all ensemble members simulate $C_h = 1 \text{ Wm}^{-2}$, but simulate $d \ln f_h / dT_s = \pm 5 \% \text{ K}^{-1}$, then their area feedbacks will range between $\pm 0.03 \text{ Wm}^{-2}\text{K}^{-1}$. This quantitative yet clear diagnostic could provide testable hypothesis that advance our understanding and development of models.

Such a physically transparent approach has even broader implications. Communicating with the public about our confidence (or lack thereof) in clouds and climate change is hard. However, a physical theory of cloud feedbacks that can constrain, quantify, and interpret models and observations, like the one proposed here, could help clear the cloud of uncertainty.

Acknowledgements

We thank Geet George for illustrating the clouds in Figure 1, and Adam Sokol, Dennis Hartmann, Marion Saint-Lu, Isla Simpson, and Bjorn Stevens for helpful conversations. B.M. was supported by the Franco-American Fulbright Commission. S.B. and J.L.D. were supported by EU Horizon 2020 grant agreement 820829 (CONSTRAIN).

412 Methods

413 **Conceptualizing cloud radiative effects** We start with an ideal-
 414 ized model of cloud radiative effects at the top of the atmosphere
 415 (TOA). Although tropical cloudiness is expected to be trimodal
 416 (60), for simplicity we will consider a domain containing two
 417 cloud types: high clouds (h) and low clouds (ℓ). (Considering
 418 mid-level clouds does not change our conclusions.) Each type has
 419 an emission temperature T_h, T_ℓ ; an optically thick cloud fraction
 420 f_h, f_ℓ ; and an albedo α_h, α_ℓ (Figure 1). Mid-level clouds will be
 421 considered in our error analysis.

422 The TOA energy balance is $N = S - R$, where S is the ab-
 423 sorbed shortwave radiation and R is the outgoing longwave ra-
 424 diation. The cloud radiative effect C is the difference in N
 425 between all-sky and clear-sky (cs) conditions, $C = N - N_{cs}$ (61).
 426 C can be decomposed into longwave and shortwave components:
 427 $C = C^{sw} + C^{lw}$.

428 In the longwave component, clear-sky regions with a surface
 429 temperature T_s will emit to space with an outgoing longwave
 430 radiation of $R_{cs}^{T_s}$, but a portion will be blocked by clouds. As-
 431 suming random overlap between high clouds and low clouds (62),
 432 the domain-averaged clear-sky contribution is $R_{cs}^{T_s}(1-f_h)(1-f_\ell)$.
 433 Low clouds are so close to the surface that we treat their emis-
 434 sion to space like clear-sky surface emission but at T_ℓ . Their
 435 domain-averaged contribution is $R_{cs}^{T_\ell}f_\ell(1-f_h)$. Since $R_{cs}^{T_s}$ is
 436 an approximately linear function of temperature (63), $R_{cs}^{T_\ell} \approx$
 437 $R_{cs}^{T_s} + \lambda_{cs}(T_s - T_\ell)$, where $\lambda_{cs} \equiv -dR_{cs}/dT_s \approx -2 \text{ Wm}^{-2}\text{K}^{-1}$ is
 438 a representative value for the longwave clear sky feedback (36).
 439 We assume that high clouds are so high that they emit directly
 440 to space (35) with a value $\sigma T_h^4 f_h$. Summing these contributions,
 441 the domain-averaged outgoing longwave radiation is

$$R = R_{cs}^{T_s}(1-f_h) + \sigma T_h^4 f_h + \lambda_{cs}(T_s - T_\ell)(1-f_h)f_\ell, \quad (13)$$

442 and the longwave cloud radiative effect $-(R - R_{cs})$ is

$$C^{lw} = R_{cs}^{T_s}f_h - \sigma T_h^4 f_h - \lambda_{cs}(T_s - T_\ell)(1-f_h)f_\ell. \quad (14)$$

443 In the shortwave component, there is an incoming solar radi-
 444 ation S^\downarrow , and we assume that there is no absorption except at
 445 the surface. High clouds reflect a portion $\alpha_h f_h$ back to space.
 446 The transmitted radiation then hits low clouds which reflect a
 447 portion $\alpha_\ell f_\ell$ back to space (ignoring secondary reflections with
 448 the anvils above). The transmitted radiation then hits the sur-
 449 face which reflects a portion α_s back out to space and absorbs
 450 the rest. Summing these contributions, the domain-averaged ab-
 451 sorbed shortwave radiation at TOA is

$$S = S^\downarrow(1 - \alpha_h f_h)(1 - \alpha_\ell f_\ell)(1 - \alpha_s). \quad (15)$$

452 The TOA absorbed shortwave in clear-skies is $S_{cs} = S^\downarrow(1 -$
 453 $\alpha_s)$, so the shortwave cloud radiative effect $(S - S_{cs})$ is:

$$C^{sw} = S_{cs}(-\alpha_h f_h - \alpha_\ell f_\ell + \alpha_h \alpha_\ell f_h f_\ell). \quad (16)$$

454 It will prove helpful to separate the contribution of high clouds
 455 and low clouds to the net cloud radiative C . Setting $f_\ell = 0$ yields
 456 the high cloud radiative effect:

$$C_h = (-S_{cs}\alpha_h + R_{cs}^{T_s} - \sigma T_h^4)f_h. \quad (17)$$

457 Setting $f_h = 0$ yields the low cloud radiative effect:

$$C_\ell = (-S_{cs}\alpha_\ell - \lambda_{cs}(T_s - T_\ell))f_\ell. \quad (18)$$

458 The total cloud radiative effect C in terms of each cloud is:

$$C = C_h + C_\ell + m_{\ell h}, \quad (19)$$

where

$$m_{\ell h} = (S_{cs}\alpha_\ell\alpha_h + \lambda_{cs}(T_s - T_\ell))f_\ell f_h, \quad (20)$$

460 represents the cloud overlap masking effect. Note that $C_h \propto$
 461 f_h , $C_\ell \propto f_\ell$, and $m_{\ell h} \propto f_\ell f_h$.

462 **Feedback decomposition** We will now derive various cloud feed-
 463 backs from these equations and assume a fixed relative humidity.
 464 The lapse rate feedback has been shown to be small when using
 465 this reference response (64, 65), so it will be ignored here.

$$\begin{aligned} \lambda &\equiv \frac{dN}{dT_s} \\ &= \frac{S_{cs}}{dT_s} - \frac{dR_{cs}^{T_s}}{dT_s} + \frac{dC}{dT_s} \\ &= \lambda_{cs}(1-f_h) \\ &\quad + (R_{cs}^{T_s} - \sigma T_h^4 + \lambda_{cs}(T_s - T_\ell)f_\ell - S_{cs}\alpha_h + S_{cs}\alpha_h\alpha_\ell f_\ell) \frac{df_h}{dT_s} \\ &\quad + (-\lambda_{cs}(T_s - T_\ell)(1-f_h) - S_{cs}\alpha_\ell + S_{cs}\alpha_h f_h \alpha_\ell) \frac{df_\ell}{dT_s} \\ &\quad + -4\sigma T_h^3 f_h \frac{dT_h}{dT_s} \\ &\quad + -\lambda_{cs}(1-f_h)f_\ell \frac{d(T_s - T_\ell)}{dT_s} \\ &\quad + (-S_{cs}f_h + S_{cs}f_h\alpha_\ell f_\ell) \frac{d\alpha_h}{dT_s} \\ &\quad + (-S_{cs}f_\ell + S_{cs}\alpha_h f_h f_\ell) \frac{d\alpha_\ell}{dT_s} \\ &\quad - S^\downarrow(1 - \alpha_h f_h)(1 - \alpha_\ell f_\ell) \frac{d\alpha_s}{dT_s} \\ &\quad - (T_s - T_\ell)(1-f_h)f_\ell \frac{d\lambda_{cs}}{dT_s}. \end{aligned} \quad (21)$$

466 Recognizing that many of these terms can be rewritten as
 467 cloud radiative effects, we get:

$$\begin{aligned} \lambda &= \lambda_{cs}(1-f_h) \\ &\quad + (C_h + m_{\ell h}) \frac{d \ln f_h}{dT_s} \\ &\quad + (C_\ell + m_{\ell h}) \frac{d \ln f_\ell}{dT_s} \\ &\quad - 4\sigma T_h^3 f_h \frac{dT_h}{dT_s} \\ &\quad - \lambda_{cs}(1-f_h)f_\ell \frac{d(T_s - T_\ell)}{dT_s} \\ &\quad + (C_h^{sw} + m_{\ell h}^{sw}) \frac{d \ln \alpha_h}{dT_s} \\ &\quad + (C_\ell^{sw} + m_{\ell h}^{sw}) \frac{d \ln \alpha_\ell}{dT_s} \\ &\quad + C_s \frac{d \ln \alpha_s}{dT_s}, \end{aligned} \quad (22)$$

468 where we have assumed that $d\lambda_{cs}/dT_s$ is negligible, and $C_s =$
 469 $-S^\downarrow(1 - \alpha_h f_h)(1 - \alpha_\ell)\alpha_s$ is the surface albedo radiative effect,
 470 which is equivalent to the ‘‘cryosphere radiative forcing’’ (66).

471 Now we name and then describe each term:

$$\lambda = \lambda_0 + \lambda_h^{\text{area}} + \lambda_\ell^{\text{area}} + \lambda_h^{\text{temp}} + \lambda_\ell^{\text{temp}} + \lambda_h^{\text{albedo}} + \lambda_\ell^{\text{albedo}} + \lambda_s^{\text{albedo}} \quad (23)$$

λ_0 is the anvil cloud-masked longwave clear-sky feedback. It is our null hypothesis for the climate response to warming because it assumes fixed relative humidity; fixed anvil temperature, area, and albedo; fixed low cloud temperature difference, area, and albedo; and fixed surface albedo. λ_h^{area} and $\lambda_\ell^{\text{area}}$ are the feedbacks from a changing anvil cloud and low cloud area, respectively. λ_h^{temp} is the feedback from a changing anvil cloud temperature. $\lambda_\ell^{\text{temp}}$ is the feedback from a changing temperature difference between low clouds and the surface. $\lambda_h^{\text{albedo}}$, $\lambda_\ell^{\text{albedo}}$, and $\lambda_s^{\text{albedo}}$ are the feedbacks from a changing albedo of anvil clouds, low clouds, and surface, respectively. We omit the surface albedo feedback from Equation 2 because we are interested in tropical climate.

Climatology We combine monthly-mean satellite observations, surface temperature measurements, and reanalysis and re-grid all datasets onto a common 2° latitude \times 2.5° longitude grid over the tropical belt (30°N – 30°S) from June 2006 to December 2016. Although anvil clouds populate the globe (67), it is less clear how extratropical anvils change with warming. Most cloud feedback assessments only consider tropical anvil clouds, so we will follow this convention.

From the CALIPSO lidar satellite dataset (37, 68), we obtain vertical profiles of cloud fraction for optical depths between $0.3 \leq \tau \leq 5$. This range excludes both deep convective cores and optically thin cirrus unconnected to deep convection (25). We then vertically smooth the native vertical 60 m resolution profiles with a 480 m running mean. For anvil detection, we consider ice cloud data above 8 km. For shallower clouds, we consider liquid cloud fraction data below 4 km. The diagnosed cloud fractions are the absolute maximum of the profile in their respective domains, but if the identified maximum does not exceed a cutoff ($f_{\text{cut}} = 0.03$), then that region is considered to be clear-sky ($f = 0$). This algorithm is applied to every grid point and then tropically-averaged. Our approach thus far resembles (25).

To match the inferred cloud radiative effects with the observed, we consider an effective cloud fraction $f_h = n \cdot \text{Max}(f(z))$ for high clouds, where n is a single tuned parameter to account for collapsing the high cloud profile into one level. This accounting is more important for high clouds, as their profile’s full width-half maximum is ≈ 5 km (Figure 1 of Extended Data), whereas low clouds are already localized with a full width-half maximum of ≈ 1 km (Figure 1 of Extended Data). While n could be more rigorously derived from detailed considerations of cloud overlap (62), we opt to determine n by fitting the predicted tropical- and time-averaged longwave cloud radiative effect C^{lw} to its observed counterpart $C_{\text{obs}}^{\text{lw}}$ from CERES (see Methods). Doing so yields a spatially and temporally constant value of $n = 1.7$. This value lies between that from assuming maximum overlap between each layer of the anvil cloud, which yields $n = 1$ and random overlap, which yields $n \approx 5$.

The height of the diagnosed cloud fraction is then used to diagnose the cloud temperatures T_h, T_ℓ at each space and time by selecting the corresponding atmospheric temperature in ERA5 reanalysis (40). We use the HadCRUT5 dataset (39) to diagnose the surface temperature T_s .

We use monthly mean TOA radiative fluxes, both clear-sky and all-sky, from the CERES satellite EBAF Ed4.1 product (38, 69). We diagnose the surface albedo α_s as the ratio of

upwelling clear-sky shortwave radiation S_{cs}^\dagger to incoming shortwave radiation S^\downarrow . However, because shortwave absorption and scattering occurs in the real atmosphere, our surface albedo is more accurately characterized as the planetary clear-sky albedo (70). We diagnose the cloud albedos by assuming that they are constant, independent of space and time, and that $\alpha_h = \alpha_\ell \equiv \alpha$. We discuss the impact of this assumption in our uncertainty analysis later on in Methods. We then infer the tropical- and time-averaged shortwave cloud radiative effect C^{sw} from Equation 16 and tune the albedo to match the observed shortwave cloud radiative effect $C_{\text{obs}}^{\text{sw}}$ from CERES. See *Cloud albedo* in Methods.

Cloud fraction We use the CALIPSO Lidar Satellite CALLID_L3_Cloud_Occurrence_Standard_V1_00 data product, the same dataset used in (25). To determine the effective cloud fraction $f_h = n \cdot \text{Max}(f(z))$, we first demand that n be constant with space and time. We then fit the predicted tropically- and temporally-averaged longwave radiative effect C^{lw} to its observed counterpart $C_{\text{obs}}^{\text{lw}}$ from CERES. Given these constraints, and the inputs to Equation 14, n can be solved for as

$$n = \frac{\langle C_{\text{obs}}^{\text{lw}} + \lambda_{cs}(T_s - T_\ell)f_\ell \rangle}{\langle R_{cs} \text{max}(f(z)) - \sigma T_h^4 \text{max}(f(z)) + \lambda_{cs}(T_s - T_\ell)f_\ell \text{max}(f(z)) \rangle}, \quad (24)$$

where $\langle \cdot \rangle$ denotes a tropical- and temporal-average.

Cloud albedo To determine the cloud albedos α_h, α_ℓ , we first demand that they equal a common value α , and then we fit the predicted tropically- and temporally-averaged shortwave cloud radiative effect C^{sw} to equal its observed counterpart $C_{\text{obs}}^{\text{sw}}$ from CERES. Given these constraints, and the inputs to Equation 16, the cloud albedo can be solved for as

$$\alpha = -\langle b \rangle - \sqrt{\frac{\langle b \rangle^2 - 4\langle a \rangle \langle c \rangle}{2\langle a \rangle}}, \quad (25)$$

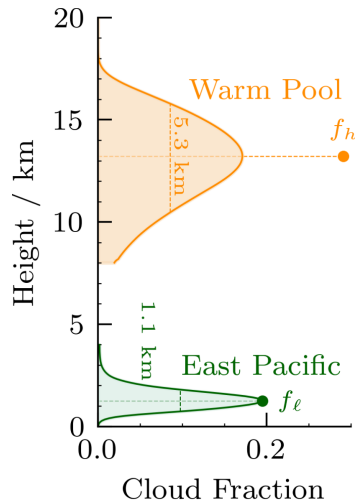
where $a = S_{cs} f_h f_\ell$, $b = -S_{cs}(f_h + f_\ell)$, $c = -C_{\text{obs}}^{\text{sw}}$.

Uncertainty analysis for area feedback Uncertainty in our estimates of $d \ln f_h / dT_s$ and $C_h + m_{\ell h}$ translate to uncertainty in λ_h^{area} . As stated in the main text, we estimate $d \ln f_h / dT_s = -4 \pm 2\% \text{ K}^{-1}$. For the anvil cloud radiative effect, we found $C_h + m_{\ell h} = -1.5 \text{ Wm}^{-2}$. However, other observational studies have found it to be -4 Wm^{-2} (44), 0.6 Wm^{-2} (19), and 2 Wm^{-2} (50). This is probably due to methodological differences and the fact that anvil clouds have no precise definition. Furthermore, CERES TOA fluxes monthly fluxes have a stated uncertainty of 2.5 Wm^{-2} (38).

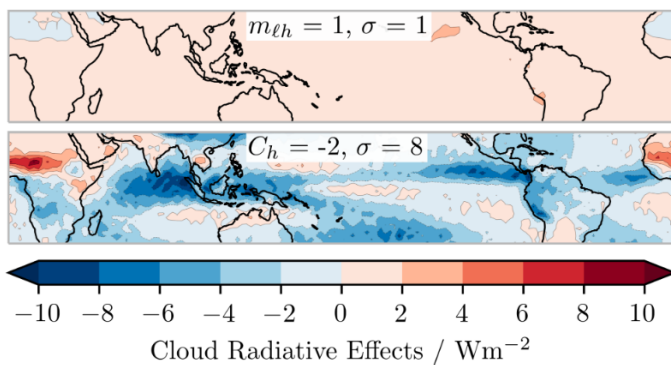
Another source of error comes from neglecting mid-level clouds, a fairly common cloud type (60). Let’s assume that emission from mid level congestus clouds (c) experience a clear-sky greenhouse effect. By symmetry with low clouds, they should contribute an additional cloud overlap masking term that appears in our expression for λ_{area} : $m_{ch} = (S_{cs} \alpha_c \alpha_h + \lambda_{cs}(T_s - T_c)) f_c f_h$. Assuming that $f_c = 0.1$, $f_h = 0.17$, $\alpha_c = \alpha_h = 0.45$, $T_c = 250 \text{ K}$, $T_s = 298 \text{ K}$, $S_{cs} = 347 \text{ Wm}^{-2}$, $\lambda_{cs} = -2 \text{ Wm}^{-1} \text{ K}^{-1}$ yields $m_{ch} \approx -0.5 \text{ Wm}^{-2}$.

We therefore estimate $C_h + m_{\ell h} = -1 \pm 3 \text{ Wm}^{-2}$. This results in our best estimate of the anvil cloud area feedback:

$$\langle \lambda_h^{\text{area}} \rangle = 1/2 \cdot (-4 \pm 2\% \text{ K}^{-1}) \cdot (-1 \pm 3 \text{ Wm}^{-2}) = 0.02 \pm 0.07 \text{ Wm}^{-2} \text{ K}^{-1}. \quad (26)$$



Extended Data Figure 1: *Illustration of effective cloud fraction.* The high cloud fraction profile in the Warm Pool and low cloud fraction profile in the East Pacific are from CALIPSO. The full width-half maximum and effective cloud fraction of each profile are shown. The high cloud and low cloud profiles are clipped below 8 km and above 4 km, respectively, in accordance with our detection method.



Extended Data Figure 2: *Climatological values of tropical quantities.* Top) Inferred cloud overlap effect from Equation 20. Bottom) Inferred anvil cloud radiative effect from Equation 17. Tropical mean values and standard deviations are shown in the upper middle of each panel. Refer to Figure 3 to see m_{lh} and C_h and other quantities plotted with a broader color scale.

References

[1] Forster, P. *et al.* Chapter 7: The Earth's energy budget, climate feedbacks, and climate sensitivity. *Intergovernmental Panel on Climate Change* (2021).

[2] Schneider, S. H. Cloudiness as a global climatic feedback mechanism: The effects on the radiation balance and surface temperature of variations in cloudiness. *Journal of Atmospheric Sciences* **29**, 1413 – 1422 (1972).

[3] Ramanathan, V. Interactions between ice-albedo, lapse-rate and cloud-top feedbacks: An analysis of the nonlinear response of a gcm climate model. *Journal of Atmospheric Sciences* **34**, 1885 – 1897 (1977).

[4] Council, N. R. *Carbon Dioxide and Climate: A Scientific Assessment* (The National Academies Press, Washington, DC, 1979).

[5] Ramanathan, V. & Collins, W. Thermodynamic regulation of ocean warming by cirrus clouds deduced from observations of the 1987 El Niño. *Nature* **351**, 27–32 (1991).

[6] Pierrehumbert, R. T. Thermostats, radiator fins, and the local runaway greenhouse. *Journal of Atmospheric Sciences* **52**, 1784 – 1806 (1995).

[7] Lindzen, R. S., Chou, M.-D. & Hou, A. Y. Does the earth have an adaptive infrared iris? *Bulletin of the American Meteorological Society* **82**, 417 – 432 (2001).

[8] Hartmann, D. L. & Michelsen, M. L. No evidence for iris. *Bulletin of the American Meteorological Society* **83**, 249 – 254 (2002).

[9] Bony, S. Comment le débat scientifique a fait progresser l'expertise sur les rétroactions atmosphériques. *Science du Changement Climatique, Acquis et Controverses* 38–42 (2004).

[10] Stephens, G. L. Cloud feedbacks in the climate system: A critical review. *Journal of Climate* **18**, 237 – 273 (2005).

[11] Mauritsen, T. & Stevens, B. Missing iris effect as a possible cause of muted hydrological change and high climate sensitivity in models. *Nature Geoscience* **8**, 8–13 (2015).

[12] Yoshimori, M., Lambert, F. H., Webb, M. J. & Andrews, T. Fixed anvil temperature feedback: Positive, zero, or negative? *Journal of Climate* **33**, 2719 – 2739 (2020).

[13] Ramanathan, V. *et al.* Cloud-radiative forcing and climate: Results from the earth radiation budget experiment. *Science* **243**, 57–63 (1989).

[14] Lau, K.-M., Sui, C.-H., Chou, M. D. & Tao, W.-K. An inquiry into the cirrus-cloud thermostat effect for tropical sea surface temperature. *Geophysical Research Letters* **21**, 1157–1160 (1994).

[15] Bony, S., Lau, K.-M. & Sud, Y. C. Sea surface temperature and large-scale circulation influences on tropical greenhouse effect and cloud radiative forcing. *Journal of Climate* **10**, 2055 – 2077 (1997).

[16] Williams, I. N., Pierrehumbert, R. T. & Huber, M. Global warming, convective threshold and false thermostats. *Geophysical Research Letters* **36** (2009).

[17] Fu, Q., Baker, M. & Hartmann, D. L. Tropical cirrus and water vapor: an effective earth infrared iris feedback? *Atmospheric Chemistry and Physics* **2**, 31–37 (2002).

[18] Lin, B., Wielicki, B. A., Chambers, L. H., Hu, Y. & Xu, K.-M. The iris hypothesis: A negative or positive cloud feedback? *Journal of Climate* **15**, 3 – 7 (2002).

[19] Gasparini, B., Blossey, P. N., Hartmann, D. L., Lin, G. & Fan, J. What drives the life cycle of tropical anvil clouds? *Journal of Advances in Modeling Earth Systems* **11**, 2586–2605 (2019).

[20] Beydoun, H., Caldwell, P. M., Hannah, W. M. & Donahue, A. S. Dissecting anvil cloud response to sea surface warming. *Geophysical Research Letters* **48**, e2021GL094049 (2021). E2021GL094049

[21] Jeevanjee, N. Three rules for the decrease of tropical convection with global warming. *Journal of Advances in Modeling Earth Systems* **14**, e2022MS003285 (2022). E2022MS003285 2022MS003285.

[22] Hartmann, D. L. & Larson, K. An important constraint on tropical cloud - climate feedback. *Geophysical Research Letters* **29**, 12–1–12–4 (2002).

[23] Zelinka, M. D. & Hartmann, D. L. Why is longwave cloud feedback positive? *Journal of Geophysical Research: Atmospheres* **115** (2010).

[24] Bony, S. *et al.* Thermodynamic control of anvil cloud amount. *Proceedings of the National Academy of Sciences* **113**, 8927–8932 (2016).

[25] Saint-Lu, M., Bony, S. & Dufresne, J.-L. Observational evidence for a stability iris effect in the tropics. *Geophysical Research Letters* **47**, e2020GL089059 (2020). E2020GL089059 10.1029/2020GL089059.

[26] Saint-Lu, M., Bony, S. & Dufresne, J.-L. Clear-sky control of anvils in response to increased CO₂ or surface warming or volcanic eruptions. *npj Climate and Atmospheric Science* **5**, 78 (2022).

[27] Ito, M. & Masunaga, H. Process-level assessment of the iris effect over tropical oceans. *Geophysical Research Letters* **49**, e2022GL097997 (2022). E2022GL097997 2022GL097997.

[28] Stauffer, C. L. & Wing, A. A. Properties, changes, and controls of deep-convecting clouds in radiative-convective equilibrium. *Journal of Advances in Modeling Earth Systems* **14**, e2021MS002917 (2022). E2021MS002917 2021MS002917.

[29] Sherwood, S. C. *et al.* An assessment of earth's climate sensitivity using multiple lines of evidence. *Reviews of Geophysics* **58**, e2019RG000678 (2020). E2019RG000678 2019RG000678.

[30] Zelinka, M. D., Klein, S. A., Qin, Y. & Myers, T. A. Evaluating climate models' cloud feedbacks against expert judgment. *Journal*

- 672 of *Geophysical Research: Atmospheres* **127**, e2021JD035198 (2022).
673 E2021JD035198 2021JD035198.
- 674 [31] Hartmann, D. L. Tropical anvil clouds and climate sensitivity. *Pro-*
675 *ceedings of the National Academy of Sciences* **113**, 8897–8899
676 (2016).
- 677 [32] Ceppi, P., Brient, F., Zelinka, M. D. & Hartmann, D. L. Cloud feed-
678 back mechanisms and their representation in global climate models.
679 *WIREs Climate Change* **8**, e465 (2017).
- 680 [33] Soden, B. J., Broccoli, A. J. & Hemler, R. S. On the use of cloud
681 forcing to estimate cloud feedback. *Journal of Climate* **17**, 3661 –
682 3665 (2004).
- 683 [34] Stevens, B., Sherwood, S. C., Bony, S. & Webb, M. J. Prospects for
684 narrowing bounds on earth's equilibrium climate sensitivity. *Earth's*
685 *Future* **4**, 512–522 (2016).
- 686 [35] *Clouds and Climate: Climate Science's Greatest Challenge* (Cam-
687 bridge University Press, 2020).
- 688 [36] McKim, B. A., Jeevanjee, N. & Vallis, G. K. Joint dependence
689 of longwave feedback on surface temperature and relative humid-
690 ity. *Geophysical Research Letters* **48**, e2021GL094074 (2021).
691 E2021GL094074 2021GL094074.
- 692 [37] Winker, D. M. *et al.* The calipso mission: A global 3d view of
693 aerosols and clouds. *Bulletin of the American Meteorological Society*
694 **91**, 1211 – 1230 (2010).
- 695 [38] Loeb, N. G. *et al.* Clouds and the earth's radiant energy system
696 (ceres) energy balanced and filled (ebaf) top-of-atmosphere (toa)
697 edition-4.0 data product. *Journal of Climate* **31**, 895 – 918 (2018).
- 698 [39] Morice, C. P. *et al.* An updated assessment of near-surface tem-
699 perature change from 1850: The hadcrut5 data set. *Journal of*
700 *Geophysical Research: Atmospheres* **126**, e2019JD032361 (2021).
701 E2019JD032361 2019JD032361.
- 702 [40] Hersbach, H. *et al.* The era5 global reanalysis. *Quarterly Journal of*
703 *the Royal Meteorological Society* **146**, 1999–2049 (2020).
- 704 [41] Hartmann, D. L. & Short, D. A. On the use of earth radiation budget
705 statistics for studies of clouds and climate. *Journal of Atmospheric*
706 *Sciences* **37**, 1233 – 1250 (1980).
- 707 [42] Harrison, E. F. *et al.* Seasonal variation of cloud radiative forc-
708 ing derived from the earth radiation budget experiment. *Journal of*
709 *Geophysical Research: Atmospheres* **95**, 18687–18703 (1990).
- 710 [43] Kiehl, J. T. On the observed near cancellation between longwave
711 and shortwave cloud forcing in tropical regions. *Journal of Climate*
712 **7**, 559 – 565 (1994).
- 713 [44] Hartmann, D. L. & Berry, S. E. The balanced radiative effect of
714 tropical anvil clouds. *Journal of Geophysical Research: Atmospheres*
715 **122**, 5003–5020 (2017).
- 716 [45] Jeevanjee, N. & Romps, D. M. Mean precipitation change from
717 a deepening troposphere. *Proceedings of the National Academy of*
718 *Sciences* **115**, 11465–11470 (2018).
- 719 [46] Wing, A. A. *et al.* Clouds and convective self-aggregation in a
720 multimodel ensemble of radiative-convective equilibrium simulations.
721 *Journal of Advances in Modeling Earth Systems* **12**, e2020MS002138
722 (2020). E2020MS002138 10.1029/2020MS002138.
- 723 [47] Fueglistaler, S. Observational evidence for two modes of coupling
724 between sea surface temperatures, tropospheric temperature profile,
725 and shortwave cloud radiative effect in the tropics. *Geophysical*
726 *Research Letters* **46**, 9890–9898 (2019).
- 727 [48] Po-Chedley, S. *et al.* Natural variability contributes to
728 model–satellite differences in tropical tropospheric warming. *Pro-*
729 *ceedings of the National Academy of Sciences* **118**, e2020962118
730 (2021).
- 731 [49] Deser, C. & Wallace, J. M. Large-scale atmospheric circulation
732 features of warm and cold episodes in the tropical pacific. *Journal*
733 *of Climate* **3**, 1254 – 1281 (1990).
- 734 [50] L'Ecuyer, T. S., Hang, Y., Matus, A. V. & Wang, Z. Reassessing the
735 effect of cloud type on earth's energy balance in the age of active
736 spaceborne observations. part i: Top of atmosphere and surface.
737 *Journal of Climate* **32**, 6197 – 6217 (2019).
- 738 [51] Kubar, T. L. & Jiang, J. H. Net cloud thinning, low-level cloud di-
739 minishment, and hadley circulation weakening of precipitating clouds
740 with tropical west pacific sst using misr and other satellite and re-
741 analysis data. *Remote Sensing* **11** (2019).
- 742 [52] Romps, D. M. An analytical model for tropical relative humidity.
743 *Journal of Climate* **27**, 7432 – 7449 (2014).
- [53] Seeley, J. T., Jeevanjee, N., Langhans, W. & Romps, D. M. For-
744 mation of tropical anvil clouds by slow evaporation. *Geophysical*
745 *Research Letters* **46**, 492–501 (2019). 746
- [54] Betts, A. K. & Harshvardhan. Thermodynamic constraint on the
747 cloud liquid water feedback in climate models. *Journal of Geophys-*
748 *ical Research: Atmospheres* **92**, 8483–8485 (1987). 749
- [55] Berry, E. & Mace, G. G. Cloud properties and radiative effects of
750 the asian summer monsoon derived from a-train data. *Journal of*
751 *Geophysical Research: Atmospheres* **119**, 9492–9508 (2014). 752
- [56] Hartmann, D. L., Moy, L. A. & Fu, Q. Tropical convection and the
753 energy balance at the top of the atmosphere. *Journal of Climate* **14**,
754 4495 – 4511 (2001). 755
- [57] Tobin, I., Bony, S. & Roca, R. Observational evidence for relation-
756 ships between the degree of aggregation of deep convection, water
757 vapor, surface fluxes, and radiation. *Journal of Climate* **25**, 6885 –
758 6904 (2012). 759
- [58] Stein, T. H. M., Holloway, C. E., Tobin, I. & Bony, S. Observed
760 relationships between cloud vertical structure and convective aggre-
761 gation over tropical ocean. *Journal of Climate* **30**, 2187 – 2207
762 (2017). 763
- [59] Bony, S. *et al.* Observed modulation of the tropical radiation bud-
764 get by deep convective organization and lower-tropospheric stabili-
765 ty. *AGU Advances* **1**, e2019AV000155 (2020). E2019AV000155
766 10.1029/2019AV000155. 767
- [60] Johnson, R. H., Rickenbach, T. M., Rutledge, S. A., Ciesielski, P. E.
768 & Schubert, W. H. Trimodal characteristics of tropical convection.
769 *Journal of Climate* **12**, 2397 – 2418 (1999). 770
- [61] Coakley, J. A. & Baldwin, D. G. Towards the objective analysis of
771 clouds from satellite imagery data. *Journal of Applied Meteorology*
772 *and Climatology* **23**, 1065 – 1099 (1984). 773
- [62] Oreopoulos, L., Cho, N. & Lee, D. Revisiting cloud overlap with a
774 merged dataset of liquid and ice cloud extinction from cloudsat and
775 calipso. *Frontiers in Remote Sensing* **3** (2022). 776
- [63] Koll, D. D. B. & Cronin, T. W. Earth's outgoing longwave
777 radiation linear due to h₂o greenhouse effect. *Proceed-*
778 *ings of the National Academy of Sciences* **115**, 10293–10298 (2018).
779 780
- [64] Held, I. M. & Shell, K. M. Using relative humidity as a state variable
781 in climate feedback analysis. *Journal of Climate* **25**, 2578 – 2582
782 (2012). 783
- [65] Zelinka, M. D. *et al.* Causes of higher climate sensitivity in cmip6
784 models. *Geophysical Research Letters* **47**, e2019GL085782 (2020).
785 E2019GL085782 10.1029/2019GL085782. 786
- [66] Flanner, M. G., Shell, K. M., Barlage, M., Perovich, D. K. &
787 Tschudi, M. A. Radiative forcing and albedo feedback from the
788 Northern Hemisphere cryosphere between 1979 and 2008. *Nature*
789 *Geoscience* **4**, 151–155 (2011). 790
- [67] Thompson, D. W. J., Bony, S. & Li, Y. Thermodynamic constraint
791 on the depth of the global tropospheric circulation. *Proceedings of*
792 *the National Academy of Sciences* **114**, 8181–8186 (2017). 793
- [68] NASA/LARC/SD/ASDC. Calipso lidar level 3 cloud occurrence
794 data, standard v1-00 (2018). 795
- [69] Loeb, N. G. *et al.* Toward a consistent definition between satellite
796 and model clear-sky radiative fluxes. *Journal of Climate* **33**, 61 – 75
797 (2020). 798
- [70] Chen, T. S. & Ohring, G. On the relationship between clear-sky
799 planetary and surfae albedos. *Journal of Atmospheric Sciences* **41**,
800 156 – 158 (1984).